THE JOURNAL OF PHYSICAL CHEMISTRY Letters

Letter

pubs.acs.org/JPCL

Thermodynamic Origin of Photoinstability in the $CH_3NH_3Pb(I_{1-x}Br_x)_3$ Hybrid Halide Perovskite Alloy

Federico Brivio,[†] Clovis Caetano,[‡] and Aron Walsh*[,†,§]

[†]Centre for Sustainable Chemical Technologies and Department of Chemistry, University of Bath, Claverton Down, Bath BA2 7AY, United Kingdom

[‡]Universidade Federal da Fronteira Sul, Realeza Paraná 85770-000, Brazil

[§]Global E[3] Institute and Department of Materials Science and Engineering, Yonsei University, Seoul 120-749, Korea

ABSTRACT: The formation of solid-solutions of iodide, bromide, and chloride provides the means to control the structure, band gap, and stability of hybrid halide perovskite semiconductors for photovoltaic applications. We report a computational investigation of the $CH_3NH_3PbI_3/CH_3NH_3PbBr_3$ alloy from density functional theory with a thermodynamic analysis performed within the generalized quasi-chemical approximation. We construct the phase diagram and identify a large miscibility gap, with a critical temperature of 343 K. The observed photoinstability in some mixed-halide solar cells is explained by the thermodynamics of alloy formation, where an initially homogeneous solution is subject to spinodal decomposition with I and Br-rich phases, which is further complicated by a wide metastable region defined by the binodal line.

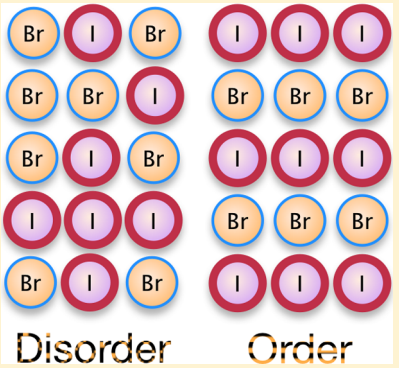

The last four years have seen the emergence of photovoltaic devices based on methylammonium lead iodide ($MAPbI_3$, MA = $CH_3NH_3^+$) and related hybrid organic−inorganic perovskites. The excitement in the field has led to a large research effort and a rapid development of high-efficiency devices.[1−3] The physical properties of $MAPbI_3$, in particular the band gap, can be tuned in several ways: (i) changing the central organic molecule MA, for example substituting it by the formamidinium (FA);[4] (ii) replacing Pb by another cation, for example Sn or Ge;[5] (iii) substituting iodine by bromine or chlorine.

The first hybrid perovskite photovoltaic devices included small amounts of chlorine, which were believed to be randomly interchanged with iodine forming the $MAPb(I_{1-x}Cl_x)_3$ pseudobinary alloy. Mixed $MAPb(I_{1-x}Br_x)_3$ has been recently successfully produced by different groups.[1,6−11] The motivating factors for the I/Br mixture are increased chemical stability and control of the band gap toward tandem solar cell applications. However, it is still not completely understood whether the alloy is stable against phase segregation in the entire range of composition. There has been some evidence for photoinduced phase separation,[12−14] which can affect measurements and performance when the material is photoexcited.[15,16] This effect is unusual, as typically electron and ion transport are decoupled (electrons move quickly with short lifetimes compared to slower ion diffusion processes). There have been some initial theoretical studies of the stability of this alloy, but they either focus on a single composition[17] or are based on the inorganic $CsPb(I_{1-x}Br_x)_3$ system.[18]

In this Letter we combine first-principles total energy calculations with a statistical mechanical treatment of the configurational space of the solid-solution formed between $MAPbI_3$ and $MAPbBr_3$. From this model, we determine how the thermodynamic potentials of the alloy vary with respect to composition and temperature. From this analysis, we construct the first phase diagram of the system. The qualitative picture that emerges is that the I/Br mixture has a miscibility gap *above* room temperature and that heavily mixed systems ($0.3 < x < 0.6$) will be subject to spinodal decomposition and phase separation at 300 K. The main two approximations in our model are the supercell expansion, which limits the configurational space of the alloy that is sampled, and the use of a pseudocubic building block, as the end member compounds and alloys show temperature-dependent structures.[6,9,19]

The calculated energy of mixing as a function of the alloy composition is shown in Figure 1. The variation is unusual, as had been already pointed out by Yin et al. for the $CsPb(I_{1-x}Br_x)_3$ alloy.[18] The $MAPb(I_{1-x}Br_x)_3$ alloy presents a large spread in the energy of mixing in the Br-rich region, which may suggest a tendency for spontaneous ordering in this region at low temperatures. Indeed, there are two configurations that have negative energies of mixing and should be stable against phase separation into the pure end-member compounds, as indicated by the convex hull in Figure 1. These configurations correspond to ordered structures of $MAPbIBr_2$ and $MAPbI_{1/2}Br_{5/2}$, as shown in Figure 2. Both structures are formed when the iodine ions are located at the apical positions, forming superlattices along the [001] direction. From the

Received: February 2, 2016
Accepted: March 7, 2016
Published: March 7, 2016

DOI: 10.1021/acs.jpclett.6b00226
J. Phys. Chem. Lett. 2016, 7, 1083−1087

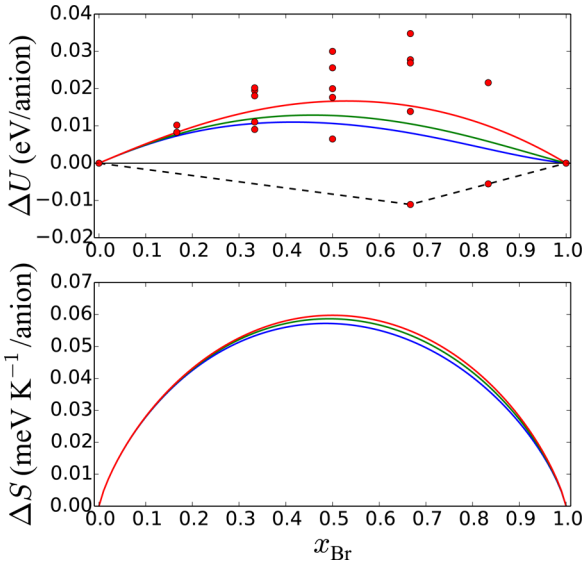

Figure 1. Energy of mixing (top) and entropy of mixing (bottom) as functions of the $CH_3NH_3Pb(I_{1-x}Br_x)_3$ alloy composition. The symbols are the values calculated for each configuration (eq 1). The solid lines show the behavior for the alloy at 200 K (blue), 300 K (green) and for a completely random alloy in the high T limit (red) within the generalized quasi-chemical approximation. The dashed line represents the convex hull.

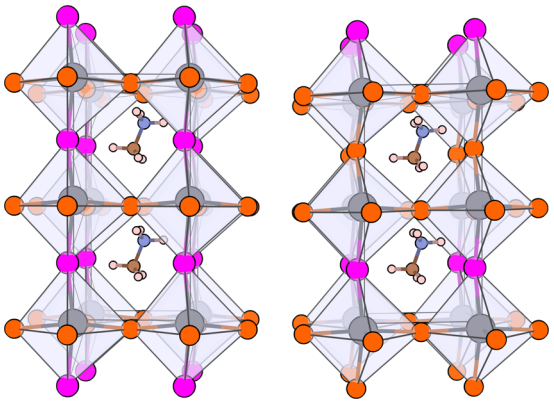

Figure 2. Stable ordered structures identified for $MAPbIBr_2$ and $MAPbI_{1/2}Br_{5/2}$, which minimize internal strain arising from the size mismatch between I and Br. The atoms at the corners of the octahedra are the halides Br (orange) and I (pink). The most stable structures are layered with iodine at the apical positions.

Shannon ionic radii,[20] the mismatch between the two halides is 0.24 Å (r_I = 2.20 Å, r_{Br} = 1.96 Å). These two ordered structures provide the structural freedom to separate the Pb−I (longer) and Pb−Br (shorter) interatomic separations along distinct directions, so that internal strain is minimized.

The variation in the energy of mixing of the alloy calculated within the generalized quasi-chemical approximation (GQCA)[21] is also shown in Figure 1. The shape of the curve changes considerably with temperature, becoming more symmetric for high temperatures. At room temperature, the energy of mixing of the solid solution can be well represented by the expression $\Omega x(1 - x)$, with $\Omega = 0.06-0.02x$ (in eV/anion), i.e., with a small deviation from the regular solution behavior. As can also be seen in Figure 1, the variation in the entropy of mixing of the alloy with temperature is close to the ideal solution expression $-k_B[x \ln x + (1 - x) \ln (1 - x)]$, which is expected for a random alloy at high temperatures. The variation of the free energy for $MAPb(I_{1-x}Br_x)_3$ is shown in Figure 3. For low temperatures the curve is asymmetric around $x = 1/2$ and is considerably lower in the Br-rich region, a consequence of the existence of the two ordered structures with negative energies of mixing described above. Also for low temperatures the free energy presents points with the same tangent, which indicates the existence of a miscibility gap. As the temperature increases, the shape of the curve becomes more symmetric as the probability of sampling all possible configurations increases.

Based on the Helmholtz free energy variation, we built the phase diagram of $MAPb(I_{1-x}Br_x)_3$, which is shown in Figure 4. The phase diagram reflects the asymmetry of the free energy, showing that the solid solution is more stable in the Br-rich region for typical growth temperatures. The phase diagram also shows that, at 300 K, the alloy is not stable against phase separation in the range of compositions between $x_1 = 0.19$ and $x_2 = 0.68$, the miscibility gap. Under equilibrium conditions, the pure compounds $MAPbI_3$ and $MAPbBr_3$ are not miscible inside this region, and two phases of compositions x_1 and x_2 must be formed. Also at room temperature, the alloy has spinodal points at the compositions $x_1' = 0.28$ and $x_2' = 0.58$, so in the intervals $x_1 < x < x_1'$ and $x_2' < x < x_2$ the alloy can present metastable phases, i.e., resistant to small fluctuations in composition. The existence of a miscibility gap at low temperatures is not a surprise, since there is a difference of 6% between the equilibrium lattice constants of $MAPbI_3$ and $MAPbBr_3$. The mismatch of the lattice constants is generally associated with the instability of isovalent solid solutions.[22] The critical temperature—the temperature above which the solid solution is stable for any composition—is 343 K, a value considerably higher than the temperature of 223 K estimated by Yin et al. for the $CsPb(I_{1-x}Br_x)_3$ perovskite.

Our model provides a simple thermodynamic explanation for the photoinduced phase separation observed in mixed halide solar cells. In an initial state, a uniform mixture can be fabricated either through control of the deposition kinetics or by annealing above the miscibility temperature. At room temperature, the uniform mixture becomes unstable, but phase separation will be a slow process. Illumination at high light intensities has the effect of overcoming these kinetic barriers and changing the local temperature. Another possible

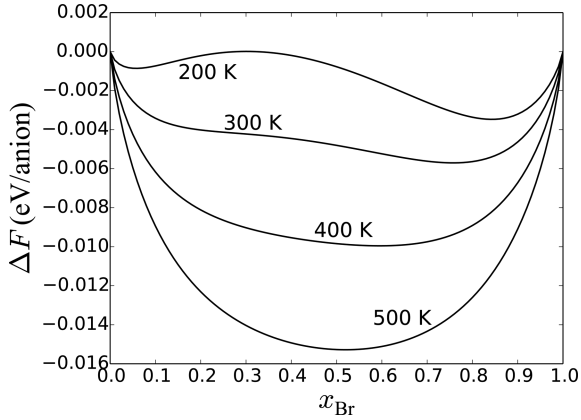

Figure 3. Calculated Helmholtz free energy as a function of the alloy composition and temperature as calculated within the generalized quasi-chemical approximation.

DOI: 10.1021/acs.jpclett.6b00226
J. Phys. Chem. Lett. 2016, 7, 1083−1087

contribution associated with the photocurrent in an active solar cell is electromigration, which will affect Br more than I due to the lower atomic mass.

Direct comparison with experiment is made difficult by the fact that most studies have reported the stoichiometry of the precursor solutions, but not the final materials. Hoke et al. investigated a range of compositions from $x = 0$ to 1, which were annealed at 373 K.[13] A blue-shift in optical absorption was found from I-rich to Br-rich compositions except for around $x = 0.5$, which showed a behavior that indicated phase separation into I-rich domains of $x \sim 0.2$ from analysis of the spectral shift in photoluminescence. Note that as Br-rich domains will have larger band gaps, they can be spectrally "invisible". The observed behavior fits very well with our predicted phase diagram (Figure 4). Upon light soaking, compositions of $x > 0.2$ were all found to exhibit decomposition to the $x \sim 0.2$ phase, which from our calculations can be interpreted as the spinodal line at 300 K. A recent investigation by Gil-Escrig of solar cells made from the Br/I mixture show a similar behavior with a marked decrease in performance for Br-rich compositions. The kinetics of these reorganization processes are consistent with the rapid anion exchange observed for these perovskites.[23,24] Low activation energies for solid-state diffusion have been predicted from simulation studies,[25−27] and there is increasing evidence for mass transport in real devices.[28,29] While it is unlikely that there is a mechanism to stabilize Br-rich mixtures toward practical devices, compositional engineering—in the three-dimensional $Cs_{1-x}MA_xPb_{1-y}Sn_yI_{3-z}Br_z$ system for example—may provide a solution to thermodynamically robust wider band gap materials.

To summarize, we have reported a statistical mechanical study of the solid-solution formed by two halide hybrid perovskites informed by quantum mechanical total energy calculations. The resulting phase diagram for $MAPb(I_{1-x}Br_x)_3$ reveals several important features: (i) a critical temperature for mixing of 343 K; (ii) a window between $0.3 < x < 0.6$ that is unstable with respect to spinodal decomposition at 300 K; (iii) a binodal (coexistence) point at $x = 0.2$ and $x = 0.7$ at 300 K. The thermodynamic metastability of this alloy for intermediate Br/I compositions explains the sensitivity of the mixture to preparatory conditions, temperature, and the operation conditions of a solar cell.

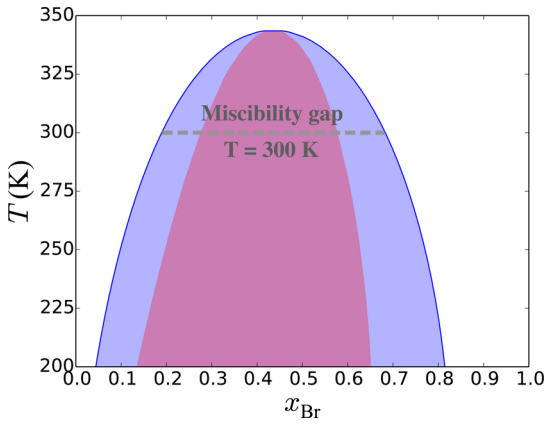

Figure 4. Predicted phase diagram of the $MAPb(I_{1-x}Br_x)_3$ alloy. The purple and pink lines are the binodal and spinodal lines, respectively. The dashed horizontal line shows the miscibility gap at room temperature. A thermodynamically stable solid-solution can be formed in the white region only.

COMPUTATIONAL METHODS

Disordered materials are challenging to accurately describe using atomistic simulations. We model the halide alloy as a statistical ensemble of independent configurations for seven compositions: $x = 0, \frac{1}{6}, \frac{1}{3}, \frac{1}{2}, \frac{2}{3}, \frac{5}{6}, 1$. The mixing energy of each configuration with energy E_j is defined as

$$\Delta U_j = E_j - (1 - x)E_{MAPbI_3} - xE_{MAPbBr_3} \quad (1)$$

where the last two terms represent fractions of the total energy of the pure compounds. The thermodynamic properties of the alloy were determined using the generalized quasi-chemical approximation.[21] This method has been successfully employed in the thermodynamic analysis of semiconductor alloys.[30,31] By taking into account the total energy and the degeneracy of each configuration, the method provides simple expressions for the mixing contribution to the alloy internal energy ΔU and the configurational entropy ΔS as functions of the composition x and temperature T accordingly to a Boltzmann distribution. With these thermodynamic potentials, the Helmholtz free energy of the alloy can be directly evaluated:

$$\Delta F(x, T) = \Delta U(x, T) - T\Delta S(x, T) \quad (2)$$

The phase diagram of the alloy can be built by calculating the free energy at different temperatures. For each temperature, the binodal points are determined by collecting the compositions for which ΔF has a common tangent. The spinodal points are those in which the second derivative of ΔF vanishes. The model has been implemented in a set of Python codes.

The configuration energies E_j were each computed within the framework of Kohn−Sham density functional theory (DFT).[32] We considered a tetragonal supercell with $2 \times 1 \times 1$ expansion of a pseudocubic perovskite building block, which corresponds to six anions.[33,34] The total number of configurations for this system is $2^6 = 64$. For a perfect inorganic cubic perovskite (O_h symmetry), the three halide sites are equivalent, which reduces the total number of configurations to 21 in total (using the SOD code[35]). Due to the presence of $CH_3NH_3^+$ cation, the symmetry is formally lowered. As a compromise between computational cost and accuracy, we take the symmetry-reduced inequivalent configurations and perform a full structural relaxation for each case. The initial cells were constructed using a linear combination of the end member lattice constants (a = 6.28 and 5.91 Å for $MAPbI_3$ and $MAPbBr_3$, respectively), i.e. Vegard's law. As the molecules are known to be rotationally active at room temperature,[36,37] a range of orientations may be accessible, but this effect is not included in our current model. Contributions from rotational and vibrational entropy are not taken into account in the free energy expansion.

For the DFT total energy calculations, we used the VASP[38] code with the Perdew−Burke−Ernzerhof exchange-correlation functional revised for solids (PBEsol)[39] and the projector augmented-wave formalism[40] including scalar-relativistic corrections. A plane-wave cutoff energy of 500 eV and a $3 \times 6 \times 6$ k-point mesh were used for all the configurations. The lattice volume and shape, and the atomic positions of each configuration were fully optimized to minimize atomic forces below 1.0 meV/Å.

Data Access Statement. The GQCA alloy code is available from https://github.com/WMD-group/GQCA_alloys and the crystal structures from https://github.com/WMD-group/hybrid-perovskites.

DOI: 10.1021/acs.jpclett.6b00226
J. Phys. Chem. Lett. 2016, 7, 1083−1087

AUTHOR INFORMATION

Corresponding Author

*E-mail: E-mail: a.walsh@bath.ac.uk.

Notes

The authors declare no competing financial interest.

ACKNOWLEDGMENTS

The simulations performed in this work benefited from membership of the UK's HPC Materials Chemistry Consortium, which is funded by EPSRC grant EP/L000202. A.W. is funded by ERC Starting Grant No. 277757, F.B. is supported by EU-FP7 Grant No. 316494, and C.C. acknowledges support from the Brazilian Research Agency CNPq Grant No. 249280/2013-2 PDE.

REFERENCES

(1) Jeon, N. J.; Noh, J. H.; Kim, Y. C.; Yang, W. S.; Ryu, S.; Seok, S. I. Solvent Engineering for High-performance Inorganic-organic Hybrid Perovskite Solar Cells. *Nat. Mater.* **2014**, *13*, 897.

(2) Zhou, H.; Chen, Q.; Li, G.; Luo, S.; Song, T.-b.; Duan, H.-S.; Hong, Z.; You, J.; Liu, Y.; Yang, Y. Interface Engineering of Highly Efficient Perovskite Solar Cells. *Science* **2014**, *345*, 542.

(3) Ahn, N.; Son, D.-Y.; Jang, I.-H.; Kang, S. M.; Choi, M.; Park, N.-G. Highly Reproducible Perovskite Solar Cells with Average Efficiency of 18.3% and Best Efficiency of 19.7% Fabricated via Lewis Base Adduct of Lead(II) Iodide. *J. Am. Chem. Soc.* **2015**, *137*, 8696.

(4) Jeon, N. J.; Noh, J. H.; Yang, W. S.; Kim, Y. C.; Ryu, S.; Seo, J.; Seok, S. I. Compositional Engineering of Perovskite Materials for High-performance Solar Cells. *Nature* **2015**, *517*, 476.

(5) Hao, F.; Stoumpos, C. C.; Chang, R. P. H.; Kanatzidis, M. G. Anomalous Band Gap Behavior in Mixed Sn and Pb Perovskites Enables Broadening of Absorption Spectrum in Solar Cells. *J. Am. Chem. Soc.* **2014**, *136*, 8094.

(6) Noh, J. H.; Im, S. H.; Heo, J. H.; Mandal, T. N.; Seok, S. I. Chemical Management for Colorful, Efficient, and Stable Inorganic-organic Hybrid Nanostructured Solar Cells. *Nano Lett.* **2013**, *13*, 1764.

(7) Sadhanala, A.; Deschler, F.; Thomas, T. H.; Dutton, S. E.; Goedel, K. C.; Hanusch, F. C.; Lai, M. L.; Steiner, U.; Bein, T.; Docampo, P.; et al. Preparation of Single Phase Films of $CH_3NH_3Pb(I_{1-x}Br_x)_3$ with Sharp Optical Band Edges. *J. Phys. Chem. Lett.* **2014**, *5*, 2501.

(8) Kulkarni, S. A.; Baikie, T.; Boix, P. P.; Yantara, N.; Mathews, N.; Mhaisalkar, S. Band-gap Tuning of Lead Halide Perovskites Using a Sequential Deposition Process. *J. Mater. Chem. A* **2014**, *2*, 9221.

(9) Fedeli, P.; Gazza, F.; Calestani, D.; Ferro, P.; Besagni, T.; Zappettini, A.; Calestani, G.; Marchi, E.; Ceroni, P.; Mosca, R. Influence of the Synthetic Procedures on the Structural and Optical Properties of Mixed-Halide (Br,I) Perovskite Films. *J. Phys. Chem. C* **2015**, *119*, 21304.

(10) Ledinský, M.; Löper, P.; Niesen, B.; Holovský, J.; Moon, S.-J.; Yum, J.-H.; De Wolf, S.; Fejfar, A.; Ballif, C. Raman Spectroscopy of Organic Inorganic Halide Perovskites. *J. Phys. Chem. Lett.* **2015**, *6*, 401.

(11) Gil-Escrig, L.; Miquel-Sempere, A.; Sessolo, M.; Bolink, H. J. Mixed Iodide-bromide Methylammonium Lead Perovskite-based Diodes for Light Emission and Photovoltaics. *J. Phys. Chem. Lett.* **2015**, *6*, 3743.

(12) Egger, D. A.; Edri, E.; Cahen, D.; Hodes, G. Perovskite Solar Cells: Do We Know What We Do Not Know? *J. Phys. Chem. Lett.* **2015**, *6*, 279.

(13) Hoke, E. T.; Slotcavage, D. J.; Dohner, E. R.; Bowring, A. R.; Karunadasa, H. I.; McGehee, M. D. Reversible Photo-induced Trap Formation in Mixed-halide Hybrid Perovskites for Photovoltaics. *Chem. Sci.* **2015**, *6*, 613.

(14) Niemann, R. G.; Kontos, A. G.; Palles, D.; Kamitsos, E. I.; Kaltzoglou, A.; Brivio, F.; Falaras, P.; Cameron, P. J. Halogen Effects on Ordering and Bonding of $CH_3NH_3^+$ in $CH_3NH_3PbX_3$ (X= Cl, Br, I) Hybrid Perovskites: A Vibrational Spectroscopic Study. *J. Phys. Chem. C* **2016**, *120*, 2509.

(15) Xiao, Z.; Yuan, Y.; Shao, Y.; Wang, Q.; Dong, Q.; Bi, C.; Sharma, P.; Gruverman, A.; Huang, J. Giant Switchable Photovoltaic Effect in Organometal Trihalide Perovskite Devices. *Nat. Mater.* **2015**, *14*, 193.

(16) Yuan, Y.; Huang, J. Ion Migration in Organometal Trihalide Perovskite and Its Impact on Photovoltaic Efficiency and Stability. *Acc. Chem. Res.* **2016**, *49*, 286.

(17) Mosconi, E.; Amat, A.; Nazeeruddin, M. K.; Grätzel, M.; De Angelis, F. First Principles Modeling of Mixed Halde Organometal Perovskites for Photovoltaic Applications. *J. Phys. Chem. C* **2013**, *117*, 13902.

(18) Yin, W.-J.; Yan, Y.; Wei, S.-H. Anomalous Alloy Properties in Mixed Halide Perovskites. *J. Phys. Chem. Lett.* **2014**, *5*, 3625.

(19) Onoda-Yamamuro, N.; Matsuo, T.; Suga, H. Calorimetric and IR Spectroscopic Studies of Phase Transitions in Methylammonium Trihalogenoplumbates (II). *J. Phys. Chem. Solids* **1990**, *51*, 1383.

(20) Shannon, R. D. Revised Effective Ionic Radii and Systematic Studies of Interatomic Distances in Halides and Chalcogenides. *Acta Crystallogr., Sect. A: Cryst. Phys., Diffr., Theor. Gen. Crystallogr.* **1976**, *32*, 751.

(21) Sher, A.; van Schilfgaarde, M.; Chen, A.-B.; Chen, W. Quasichemical Approximation in Binary Alloys. *Phys. Rev. B: Condens. Matter Mater. Phys.* **1987**, *36*, 4279.

(22) Stringfellow, G. Calculation of Ternary and Quaternary III-V Phase Diagrams. *J. Cryst. Growth* **1974**, *27*, 21.

(23) Yang, T.-Y.; Gregori, G.; Pellet, N.; Grätzel, M.; Maier, J. The Significance of Ion Conduction in a Hybrid Organic-Inorganic Lead-Iodide-Based Perovskite Photosensitizer. *Angew. Chem., Int. Ed.* **2015**, *54*, 7905.

(24) Zhang, Y.; Liu, M.; Eperon, G. E.; Leijtens, T. C.; McMeekin, D.; Saliba, M.; Zhang, W.; De Bastiani, M.; Petrozza, A.; Herz, L. M.; et al. Charge Selective Contacts, Mobile Ions and Anomalous Hysteresis in Organic-Inorganic Perovskite Solar Cells. *Mater. Horiz.* **2015**, *2*, 315.

(25) Eames, C.; Frost, J. M.; Barnes, P. R. F.; O'Regan, B. C.; Walsh, A.; Islam, M. S. Ionic Transport in Hybrid Lead Iodide Perovskite Solar Cells. *Nat. Commun.* **2015**, *6*, 7497.

(26) Haruyama, J.; Sodeyama, K.; Han, L.; Tateyama, Y. First-Principles Study of Ion Diffusion in Perovskite Solar Cell Sensitizers. *J. Am. Chem. Soc.* **2015**, *137*, 10048.

(27) Azpiroz, J. M.; Mosconi, E.; Bisquert, J.; De Angelis, F. Defects Migration in Methylammonium Lead Iodide and their Role in Perovskite Solar Cells Operation. *Energy Environ. Sci.* **2015**, *8*, 2118.

(28) Hentz, O.; Zhao, Z.; Gradecak, S. Impacts of Ion Segregation on Local Optical Properties in Mixed Halide Perovskite Films. *Nano Lett.* **2016**, *16*, 1485.

(29) Shi, J.; Xu, X.; Zhang, H.; Luo, Y.; Li, D.; Meng, Q. Intrinsic Slow Charge Response in the Perovskite Solar Cells: Electron and Ion Transport. *Appl. Phys. Lett.* **2015**, *107*, 163901.

(30) Teles, L. K.; Furthmüller, J.; Scolfaro, L. M. R.; Leite, J. R.; Bechstedt, F. First-principles Calculations of the Thermodynamic and Structural Properties of Strained $In_xGa_{1-x}N$ and $Al_xGa_{1-x}N$ Alloys. *Phys. Rev. B: Condens. Matter Mater. Phys.* **2000**, *62*, 2475.

(31) Schleife, A.; Eisenacher, M.; Rödl, C.; Fuchs, F.; Furthmüller, J.; Bechstedt, F. Ab initio Description of Heterostructural Alloys: Thermodynamic and Structural Properties of $Mg_xZn_{1-x}O$ and $Cd_xZn_{1-x}O$. *Phys. Rev. B: Condens. Matter Mater. Phys.* **2010**, *81*, 245210.

(32) Kohn, W.; Sham, L. J. Self-consistent Equations Including Exchange and Correlation Effects. *Phys. Rev.* **1965**, *140*, A1133.

(33) Frost, J. M.; Butler, K. T.; Brivio, F.; Hendon, C. H.; van Schilfgaarde, M.; Walsh, A. Atomistic Origins of High-Performance in Hybrid Halide Perovskite Solar Cells. *Nano Lett.* **2014**, *14*, 2584.

(34) Brivio, F.; Frost, J. M.; Skelton, J. M.; Jackson, A. J.; Weber, O. J.; Weller, M. T.; Goni, A. R.; Leguy, A. M. A.; Barnes, P. R. F.; Walsh, A. Lattice Dynamics and Vibrational Spectra of the Orthorhombic,

DOI: 10.1021/acs.jpclett.6b00226
J. Phys. Chem. Lett. 2016, 7, 1083−1087

Tetragonal, and Cubic Phases of Methylammonium Lead Iodide. *Phys. Rev. B: Condens. Matter Mater. Phys.* **2015**, *92*, 144308.
(35) Grau-Crespo, R.; Hamad, S.; Catlow, C. R. A.; de Leeuw, N. H. Symmetry-adapted Configurational Modelling of Fractional Site Occupancy in Solids. *J. Phys.: Condens. Matter* **2007**, *19*, 256201.
(36) Leguy, A.; Hu, Y.; Campoy-Quiles, M.; Alonso, M. I.; Weber, O. J.; Azarhoosh, P.; van Schilfgaarde, M.; Weller, M. T.; Bein, T.; Nelson, J.; et al. The Reversible Hydration of $CH_3NH_3PbI_3$ in Films, Single Crystals and Solar Cells. *Chem. Mater.* **2015**, *27*, 3397.
(37) Bakulin, A. A.; Selig, O.; Bakker, H. J.; Rezus, Y. L. A.; Müller, C.; Glaser, T.; Lovrincic, R.; Sun, Z.; Chen, Z.; Walsh, A.; et al. Real-Time Observation of Organic Cation Reorientation in Methylammonium Lead Iodide Perovskites. *J. Phys. Chem. Lett.* **2015**, *6*, 3663.
(38) Kresse, G.; Furthmüller, J. Efficient Iterative Schemes for Ab initio Total-energy Calculations Using a Plane-wave Basis Set. *Phys. Rev. B: Condens. Matter Mater. Phys.* **1996**, *54*, 11169.
(39) Perdew, J. P.; Ruzsinszky, A.; Csonka, G. I.; Vydrov, O. A.; Scuseria, G. E.; Constantin, L. A.; Zhou, X.; Burke, K. Restoring the Density-Gradient Expansion for Exchange in Solids and Surfaces. *Phys. Rev. Lett.* **2008**, *100*, 136406.
(40) Blöchl, P. E. Projector Augmented-wave Method. *Phys. Rev. B: Condens. Matter Mater. Phys.* **1994**, *50*, 17953.

DOI: 10.1021/acs.jpclett.6b00226
J. Phys. Chem. Lett. 2016, 7, 1083−1087